

Monte Carlo and DFT calculations on the corrosion inhibition efficiency of some benzimide molecules

Dyari Mustafa Mamand¹, Yousif Hussein Azeez², Hiwa Mohammad Qadr¹

¹ University of Raparin, College of Science, Department of Physics, Sulaymaniyah, Iraq

² Halabja University, College of Science, Department of Physics, Halabja, Iraq

*Author to whom correspondence should be addressed

Hiwa Mohammad Qadr

University of Raparin
College of Science
Department of Physics
Sulaymaniyah, Iraq

E-mail: hiwa.physics@uor.edu.krd

ORCID: [0000-0001-5585-3260](https://orcid.org/0000-0001-5585-3260)

This article has been accepted for publication and undergone full peer review but has not been through the copyediting, typesetting, and proofreading process, which may lead to differences between this version and the official version of record.

Please cite this article as: Mamand D.M, Azeez Y.S, Qadr H.M. Monte Carlo and DFT calculations on the corrosion inhibition efficiency of some benzimide molecules. *Mongolian Journal of Chemistry*, **24**(50), 2023, xx

<https://doi.org/10.5564/mjc.v24i50.2435>

Monte Carlo and DFT calculations on the corrosion inhibition efficiency of some benzimide molecules

3 Dyari Mustafa Mamand¹, <https://orcid.org/0000-0002-1215-7094>

Yousif Hussein Azeez²

Hiwa Mohammad Qadr¹, <https://orcid.org/0000-0001-5585-3260>

6 ¹University of Raparin, College of Science, Department of Physics, Sulaymaniyah, Iraq

²Halabja University, College of Science, Department of Physics, Halabja, Iraq

ABSTRACT

9 Calculations using density functional theory (DFT) and Monte Carlo methods were performed on 2-methylbenzimidazole, 2-mercaptobenzimidazole, 2-aminobenzimidazole, benzotriazole, and benzimidazole to determine their corrosion inhibition efficiency. The
12 molecular structure was optimized geometrically using DFT calculations at the B3LYP/6–311 G++(d,p) and b2plypd3/aug-cc-pvdz basis set level in protonated and non-protonated species in gas and water. In this study, HOMO, LUMO, bandgap, ionization energy,
15 electronegativity, hardness, softness, electrophilicity and nucleophilicity, electron transfer, back donation energy and condensed Fukui indices are used to assess a molecule's local reactivity. Theoretical investigations can precisely establish the geometrical dimensions of
18 a molecule and correctly explain the quantum properties of inhibitors. The mechanism of interaction between inhibitors and metal surfaces in a specified molecule is studied using molecular dynamics. The benzimidazole functional groups absorbed energy linearly on
21 metal surfaces, with quantum characteristics determined using density functional theory and an ab initio technique. Importantly, the findings of this conceptual model are consistent with the corrosion inhibition efficiency of earlier experimental investigations.

24 **Keywords:** DFT, Monte Carlo, benzimide, corrosion

27 INTRODUCTION

The oxide layer in metals causes structural deterioration. Corrosion conditions, such as hydrochloric acid and nitric acid, typically activate this reaction [1, 2]. Corrosion is a complex process to overcome, and if left uncontrolled, it can cause high economic losses. As a result, considerable research is already being conducted to identify corrosion inhibitors that are ecologically benign, inexpensive, and efficient [3, 4]. Natural organic molecules have a strong potential for development as corrosion inhibitors. This molecule was chosen as a corrosion inhibitor because it fits the requirements of high efficiency, low cost, environmental friendliness, non-toxicity, and no hazardous pollutants. Several experimental studies on the corrosion inhibition efficacy of organic product molecules have been conducted. Alkaloids derived from natural products, for instance, have great potential as corrosion inhibitors. The main mechanisms that limit corrosion are related to electron acceptors, electrostatic interactions, electron donors, and heteroatom groups on inhibitor molecules. In the alkaloid structure, heterocyclic benzene and heteroatom groups such as Nitrogen, Sulphur, Oxygen and heteroatoms perform roles as electron donors, electrostatic interactions, and the metal surface interactions with electron donor acceptors. The inhibitor will use these characteristics to get securely adhered to the metal surface and build a thin coating that will prevent the pace of corrosion.

2-Methylbenzimidazole is a significant pharmacophore that is frequently utilized in biomedical sciences to synthesize a variety of antibacterial and antifungal drugs. It can serve as a crucial precursor in the synthesis of substituted benzimidazole [5, 6]. 2-mercaptobenzimidazole is frequently utilized as a rubber accelerator and as an antioxidant for rubber and plastics. 2-Mercaptobenzimidazole and its products are insecticides, and it is also a prominent analytical reagent for mercury, had been used to determine Cd(II), Cu(II) and Fe(II) metal ions in industrial wastewater samples and sewage water [7-9]. As antibiofilm agents, 2-aminobenzimidazole and its derivatives have been produced. Several studies have shown that 2-aminobenzimidazole may selectively suppress and disperse Gram-positive and Gram-negative bacterial biofilms without affecting free germ cell growth. A no microbicidal chemical that affects biofilm formation may be used as an additional ingredient in an antibiofilm approach. Because even if a chemical efficiently suppresses biofilm formation without killing the microbial cells, planktonic cells can attach to other sites and form a biofilm. As a result, 2-aminobenzimidazole derivatives and antibiotics are effective against bacterial biofilms [10]. Benzimidazole and its derivatives are recognized as a major heterocyclic motif with several pharmacological uses, especially anti-diabetics, anti-

cancer, anti-convulsant, antivirals, antifungals, anti-hypertensives and anti-HIVs [11]. Because of its anti-mycobacterial characteristics, benzotriazole is appealing as a heterocycle [12]. Corrosion inhibitors are among the most extensively used and cost-effective techniques for preventing corrosion in metals and alloys. Typical corrosion inhibitors are bio-toxic chemical substances with substantial toxicity problems. Drugs are mostly used as corrosion inhibitors. The use of pharmaceuticals as corrosion inhibitors of metal corrosion has some advantages over the use of various inorganic/organic inhibitors due to their low or negligible impact on the environment. Because the drugs are harmless, inexpensive, and have minor environmental consequences, it is best to replace the current corrosion-damaging inhibitor. Many of those skilled in the art feel that the drugs are corrosion inhibitors that can compare favorably with identified green rust inhibitors and that most of these drugs, can be synthesized from natural compounds.

In this study, great attention has been paid to the electronic structure and chemical properties of each inhibitor shown in Fig. 1: 2-methylbenzimidazole, 2-mercapto benzimidazole, 2-aminobenzimidazole, benzotriazole and benzimidazole. Through their use, we were able to reach a conclusion that is consistent with previous experimental results regarding their ability to prevent corrosion.

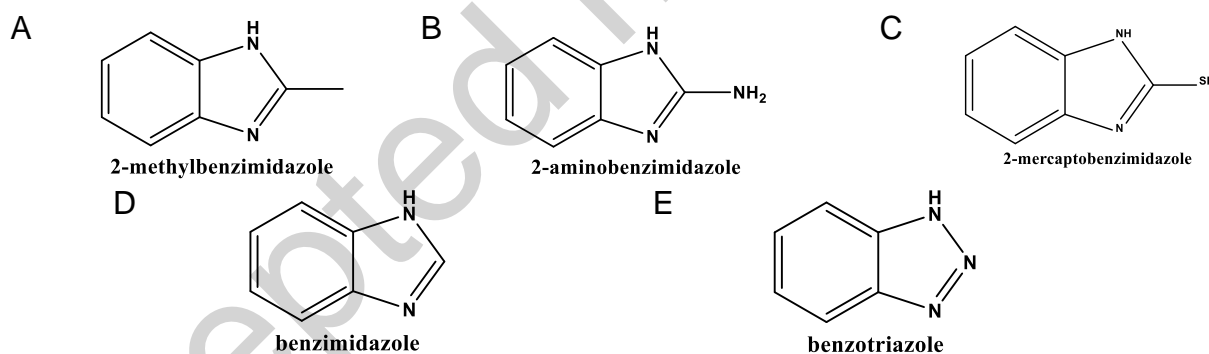


Fig. 1. Chemical structures of all inhibitors

Computational detail: The quantum chemical calculations have been carried out at DFT (B3LYP) methods with 6-311++G (d, p) and b2plypd3/aug-cc-pvdz with Gaussian09 software [13, 14]. Because electrochemical corrosion occurs in the liquid phase, including the influence of solvent is computationally feasible. The calculations in the solution were carried out using the self-consistent reaction field (SCRF) concept and Tomasi's polarized continuum model (PCM) [15]. These approaches describe the cavity in which the solute is inserted as a uniform sequence of interconnecting atomic spheres and model the solution

as a continuum of uniform dielectric constant (DC= 78.5). As well as, the Fukui functions
 90 and the thermodynamic parameters were tabulated. Kinetic stability and chemical reactivity
 properties of the optimized molecular structure have been found by the frontier molecular
 orbitals (FMOs).

93 RESULTS AND DISCUSSION

DFT with Global Chemical Reactivity Descriptors: The global reactivity indices provide
 information on a chemical compound's stability, reactivity, and selectivity. Global reactivity
 96 characteristics such as energy gap (E_g), global hardness (η), global softness (S),
 electronegativity (χ), chemical potential (μ), maximal amount of electronic charge (Q^{max}),
 electrophilicity (ω), electrodonating power (ω^-), electroaccepting power (ω^+), and net
 99 electrophilicity based on DFT with 6311++G (d,p) and b2plypd3/aug-cc-pvdz were
 calculated by using the energies of the frontier orbitals and Gaussian 09 software (1-10)
 [16-19].

$$IP = -E_{HOMO} \quad \text{and} \quad EA = -E_{LUMO} \quad (1)$$

$$E_g = E_{LUMO} - E_{HOMO} \quad (2)$$

$$\chi = \frac{E_{HOMO} + E_{LUMO}}{2} \quad (3)$$

$$\mu = -\frac{(E_{HOMO} + E_{LUMO})}{2} \quad (4)$$

$$\eta = \frac{E_{LUMO} - E_{HOMO}}{2} \quad (5)$$

$$S = \frac{1}{2\eta} \quad (6)$$

$$\omega = \frac{\mu^2}{2\eta} \quad (7)$$

$$\Delta N = \frac{\chi_{cu} - \chi_{inh}}{2 \sum \eta_{cu} - \eta_{inh}} \quad (8)$$

$$\varepsilon = \frac{1}{\omega} \quad (9)$$

$$\Delta E_{back-donation} = \frac{-\eta}{4} \quad (10)$$

102 **Fukui Function (local reactivity descriptors):** The Fukui Function gives information on
 the reactivity indices in a given system. For the highest Fukui function values, the atom
 exhibits a significant degree of reactivity. The Fukui functions from (compound 1-5) has
 105 been calculated on the basis of B3LYP/6-311++G(d,p) and b2plypd3/aug-cc-pvdz level of

theory, and the results are shown in Tables 1-4. The Fukui Functions (f_k^-, f_k^+) are computed using Mulliken population analysis charges of negative and positive ions and are given in
108 Tables 7, 9, 11, and 13 using equations 11 and 12. If (N) represents the number of electrons, then (N + 1) denotes an anion and (N – 1) denotes the system's cation [20].

$$f_k^+ = q(N + 1) - q(N) \quad (11)$$

$$f_k^- = q(N) - q(N - 1) \quad (12)$$

111 **Quantum chemical parameters:** Quantum chemical calculations have long been used to study reaction processes. They have very effective tools for studying metal corrosion inhibition [21, 22]. The electrostatics and spatial molecules of a corrosion inhibition efficiency
114 are directly related to its performance, the relationships between quantum chemical properties and inhibitory effect studied in this work. The calculation of quantum chemical parameters in corrosion inhibition investigations includes two basic characteristics: first,
117 identifying the correlation between inhibitor molecular structure and inhibitory behavior; and second, developing a hypothesized inhibition mechanism in terms of chemical reactivity of compounds [23]. In addition, quantum chemical descriptor variables were related to
120 experimental values to explore inhibitor molecular reactivity. The frontier molecular orbitals (E_{HOMO} , E_{LUMO}) and quantum chemical indices such as molecular hardness, molecular softness, electronegativity, and chemical potential are tabulated in Tables 1-4. Interaction
123 between reacting species occurs through FMOs (E_{HOMO} and E_{LUMO}). Furthermore, ionization potential (IP) = E_{HOMO} relates to the capacity of the inhibitor to donate electrons and indicates the electron-donating propensity of the molecule. Thus, higher value of E_{HOMO} signifies
126 better propensity of donating electron, and enhancing the adsorption of the inhibitor on the metal surface and so better inhibition performance. E_{LUMO} energy is connected to electron affinity (EA) = E_{LUMO} and shows the ability of a molecule to receive electrons. Thus, better
129 capacity to receive electrons is indicated by a lower value of E_{LUMO} , which will also improve the adsorption of the inhibitor on the metal surface and therefore improve inhibition effectiveness [24]. As can be seen in Tables 1 and 3, the greatest value of E_{HOMO} and the
132 lowest value of E_{LUMO} for the caffeine compound compared to other findings in gas phase and solvent phase (water) show that 2-methylbenzimidazol has a higher inhibitory efficiency, which is consistent with the experimental result.

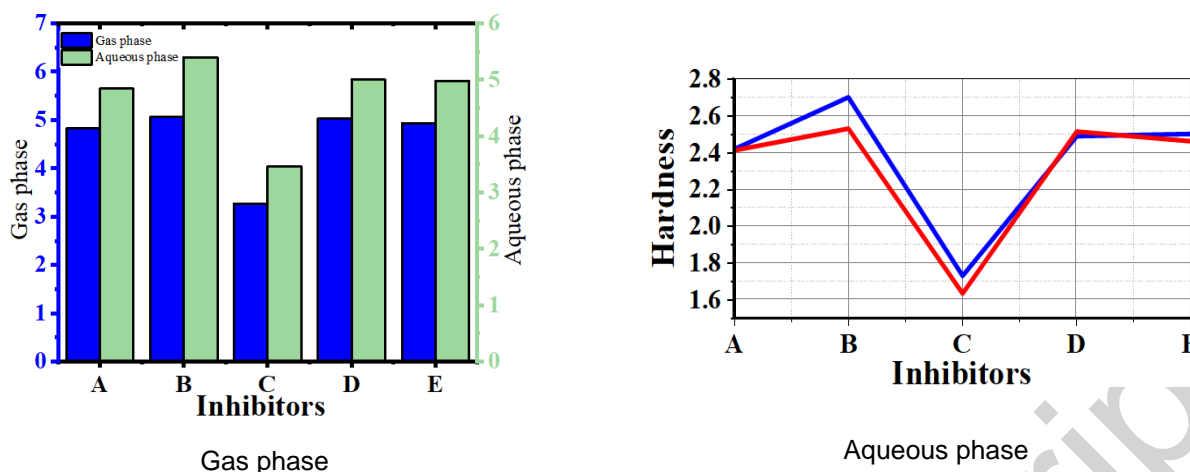


Fig. 2. Bandgap and harness of selected inhibitors in gas and aqueous phase

138 The ionization energy of an element is the ability of materials to participate in chemical
 processes that require ion creation or electron donation. It is also often connected to the
 type of chemical bonding in the elements' complexes [25]. The ionization potential of an
 141 inhibitor can be used to determine its reactivity. As displayed in Tables 1-4, a high ionization
 potential value implies that the compound is very reactive, whereas a low ionization potential
 value suggests that the molecule is inactive. 2-amino benzimidazole has the highest
 144 corrosion inhibition efficiency.

The frontier energy gap between E_{HOMO} and E_{LUMO} is an essential characteristic for inhibitor
 molecule adsorption on metallic surfaces. Lower energy differences improve inhibition
 147 efficiency and reactivity, because it takes less energy to remove an electron from the last
 occupied orbital. The 2-methylbenzimidazol inhibitor has the smallest energy gap compared
 to other compounds, as shown in Fig. 2 and Tables 1 and 4. This suggests that the 2-
 150 mercaptobenzimidazol molecule may have superior performance compared to the other
 molecule, a conclusion that is consistent with the experimental result.

The global hardness and softness are significant for evaluating the stability and reactivity of
 153 molecules. Hard molecules have big energy gaps whereas soft molecules have small ones
 [26]. Our results in Tables 1, 3 and Fig. 2, A and B reveals that, 2-mercapto benzimidazole
 and 2-methylbenzimidazol has low hardness than the rest of molecules in gas phase and
 156 solvent phase. The inhibitor with the lowest absolute hardness value is predicted to be the
 most effective in inhibiting a target molecule. 2-methylbenzimidazol and benzotriazole have
 a greater softness than other compounds in gas and solvent medium.

159 Electronegativity (χ) is another characteristic of inhibitory efficiency, and electronegativity
 values found for the evaluated inhibitor molecules may offer information about the covalent
 interactions between the inhibitor and the metal surface [27, 28]. According to the data in

162 Tables 1-4, 2-mercaptobenzimidazole and 2-methylbenzimidazol has the lowest absolute
 electronegativity (maximum chemical potential). 2-mercaptobenzimidazole and 2-
 165 methylbenzimidazol has a higher inhibitory effectiveness due to its low electronegativity and
 high chemical potential. 2-aminobenzimidazole has the lowest corrosion inhibition efficiency
 compare with all other inhibitors in this study.

Nucleophilicity and electrophilicity are plausible quantum chemical variables for predicting
 168 molecule chemical behavior. These values can be used to evaluate inhibitor performance
 [27]. It should be mentioned that a compound with a high electrophilicity value is useless for
 corrosion inhibition. In contrast, 2-mercaptobenzimidazol, which has a high nucleophilicity
 171 value, is an excellent corrosion inhibitor [28].

When Fe and inhibitor are combined, electrons flow from inhibitor to Fe until the chemical
 potential is equal. The fraction of electrons transferred ΔN , computed by considering the
 174 absolute electronegativity of iron ($\chi_{Fe} = 7 \text{ eV}$) and global hardness ($\eta_{Fe} = 0$), assuming
 metallic bulk IP = EA [29]. When ΔN is less than 3.6, the capacity of the compounds
 (inhibitors) to donate electrons to the metal surface increases the inhibition efficiency. In our
 177 investigation, inhibition efficiency also increased as ΔN values increased [30]. Therefore,
 the highest fraction of transferred electrons is related with the most effective inhibitor (2-
 mercaptobenzimidazole), whereas the lowest fraction is associated with the least effective
 180 inhibitor (2-aminobenzimidazole).

Tables 1 to 4 also includes the computed $E_{\text{Back-donation}}$ values for the all the compounds
 (inhibitors) in gas phase and in water solvent. The reverse donation of charges is the
 183 negative of hardness ($-\eta/4$) in the presence of charge transfer, which governs the interaction
 between the inhibitors and the metal surface. The $E_{\text{Back-donation}}$ suggests that charge transfer
 to a molecule, followed by a back-donation from the molecule, is energetically favored, when
 186 $\eta > 0$ and $E_{\text{Back-donation}} < 0$. Consequently, the following sequence is observed: 2-
 mercaptobenzimidazole > 2-methylbenzimidazol > benzimidazole > benzotriazole > 2-
 aminobenzimidazole, indicating that back donation is preferred for the 2-
 189 methylbenzimidazol, which is the most effective inhibitor.

Table 1. Quantum chemical parameters in gas phase at B3LYP/6-311 G++(d,p)

Indices	2- amino benzimidazole	2-methyl benzimidazol	2-mercapto benzimidazole	benzimidazole	benzotriazole
E_{HOMO} (eV)	-5.842	-5.369	-5.91	-5.461	-6.282
E_{LUMO} (eV)	-0.781	-0.544	-0.639	-0.536	-1.252
IP (eV)	5.842	5.369	3.91	5.461	6.282
EA (eV)	0.781	0.544	0.639	0.536	1.252
E_g (eV)	5.061	4.825	3.271	4.925	5.03

η (eV)	2.531	2.413	1.6355	2.4625	2.515
S (eV) ⁻¹	0.198	0.207	0.611434	0.406091	0.397614
χ (eV)	3.312	2.957	2.2745	2.9985	3.767
μ (eV)	-3.312	-2.957	-2.2745	-2.9985	-3.767
ω (eV)	2.167	1.812	1.581581	1.825584	2.821131
ε (eV) ⁻¹	0.461	0.552	0.632279	0.54777	0.354468
ΔN	0.330	0.419	1.444665	0.812487	0.642744
$\Delta E_{back-donation}$ (eV)	-0.63275	-0.60325	-0.40888	-0.61563	-0.62875

192 Table 2. Quantum chemical parameters in gas phase at b2plypd3/aug-cc-pvdz

Indices	2- amino benzimidazole	2-methyl benzimidazol	2-mercapto benzimidazole	benzimidazole	benzotriazole
E_{HOMO} (eV)	-6.241	-7.047	-6.627	-7.231	-7.789
E_{LUMO} (eV)	-1.678	-2.516	-3.203	-0.602	-0.126
IP (eV)	6.241	7.047	6.627	7.231	7.789
EA (eV)	1.678	2.516	3.203	0.602	0.126
E_g (eV)	4.563	4.531	3.424	6.629	7.663
η (eV)	2.2815	2.265	1.712	3.3145	3.8315
S (eV) ⁻¹	0.219	0.441	0.584	0.151	0.130
χ (eV)	3.9595	4.781	4.915	3.9165	3.9575
μ (eV)	-3.9595	-4.781	-4.915	-3.9165	-3.9575
ω (eV)	3.436	5.045	7.055	2.314	2.044
ε (eV) ⁻¹	0.291	0.198	0.141	0.432	0.489
ΔN	1.735	-0.566	-0.428	1.182	1.033
$\Delta E_{back-donation}$ (eV)	-0.570	0.489	0.608	-0.829	-0.958

Table 3. Quantum chemical parameters in aqueous medium at B3LYP/6-311 G++(d,p)

Indices	2- amino benzimidazole	2-methyl benzimidazol	2-mercapto benzimidazole	benzimidazole	benzotriazole
E_{HOMO} (eV)	-7.247	-7.047	-6.871	-7.231	-7.778
E_{LUMO} (eV)	-0.615	-0.516	-0.246	-0.602	-0.197
IP (eV)	7.247	7.047	6.871	7.231	7.778
EA (eV)	0.615	0.516	0.246	0.602	0.197
E_g (eV)	6.632	6.531	6.625	6.629	7.581
η (eV)	3.316	3.2655	3.3125	3.3145	3.7905
S (eV) ⁻¹	0.151	0.153	0.151	0.151	0.132
χ (eV)	3.931	3.7815	3.5585	3.9165	3.9875
μ (eV)	-3.931	-3.7815	-3.5585	-3.9165	-3.9875
ω (eV)	2.330	2.190	1.911	2.314	2.097
ε (eV) ⁻¹	0.429	0.457	0.523	0.432	0.477
ΔN	1.185	1.158	1.074	1.182	1.052
$\Delta E_{back-donation}$ (eV)	-0.829	-0.816	-0.828	-0.829	-0.948

195

Table 4. Quantum chemical parameters in aqueous medium at b2plypd3/aug-cc-pvdz

Indices	2- amino benzimidazole	2-methyl benzimidazol	2-mercapto benzimidazole	benzimidazole	benzotriazole
E_{HOMO} (eV)	-5.767	-6.531	-4.151	-5.772	-6.431
E_{LUMO} (eV)	-0.365	-1.692	-0.689	-0.791	-1.427
IP (eV)	5.767	6.531	4.151	5.772	6.431
EA (eV)	0.365	1.692	0.689	0.791	1.427
E_g (eV)	5.402	4.839	3.462	4.981	5.004
η (eV)	2.701	2.4195	1.731	2.4905	2.502
S (eV) ⁻¹	0.185	0.207	0.577701	0.401526	0.200
χ (eV)	3.066	4.112	2.42	3.2815	3.929
μ (eV)	-3.066	-4.112	-2.42	-3.2815	-3.929
ω (eV)	1.740	3.493	1.691623	2.161864	3.085
ε (eV) ⁻¹	0.575	0.286	0.591148	0.462564	0.324
ΔN	0.354	0.179	1.322935	0.746537	0.210
$\Delta E_{\text{back-donation}}$ (eV)	-0.675	-0.605	-0.43275	-0.62263	-0.626

198 **Dipole moment:** Another unique feature indicated in Tables 5 and 6 are the dipole moment
in gas and aqueous phases. While prior research has not revealed a significant relationship
between dipole moment and corrosion inhibition efficiency, the inhibitory efficiency shows
201 that a large dipole moment indicates high corrosion inhibition potency [18, 31]. Several
research revealed that decreasing the dipole moment value promoted corrosion. The dipole
moment (μ) is a polarity measurement for a polar covalent bond. It is computed as the total
204 of the atom charges and the distance between the two bound atoms [32]. Therefore, the
total dipole moment only represents a molecule's global polarity. For a perfect nucleus, the
vector sum of the individual bond dipole moments may be used to estimate the sum of the
207 molecular dipole moments. However, a high dipole moment indicates a low bandgap and
high softness, which increases the inhibition ability of the material as shown in Tables 5 and
6. The ranking of materials used for corrosion on this parameter is as follows: 2-
210 mercaptobenzimidazole > 2-methylbenzimidazol > benzotriazole > 2-aminobenzimidazole.

213 Table 5. Dipole moments in gas phase and aqueous at B3LYP/6-311 G++(d,p)

Dipole moment (Debye)	2-methyl benzimidazol	2- amino benzimidazole	2-mercapto benzimidazole	benzimidazole	benzotriazole
Gas phase	3.555	3.272	3.855	3.482	3.398
Water	5.624	4.176	5.904	5.586	5.202

Table 6. Dipole moments in gas phase and aqueous at b2plypd3/aug-cc-pvdz

Dipole moment (Debye)	2-methyl benzimidazol	2- amino benzimidazole	2-mercapto benzimidazole	benzimidazole	benzotriazole
Gas phase	4.708	3.580	5.034	3.642	4.251
Water	6.279	5.028	7.454	5.961	5.778

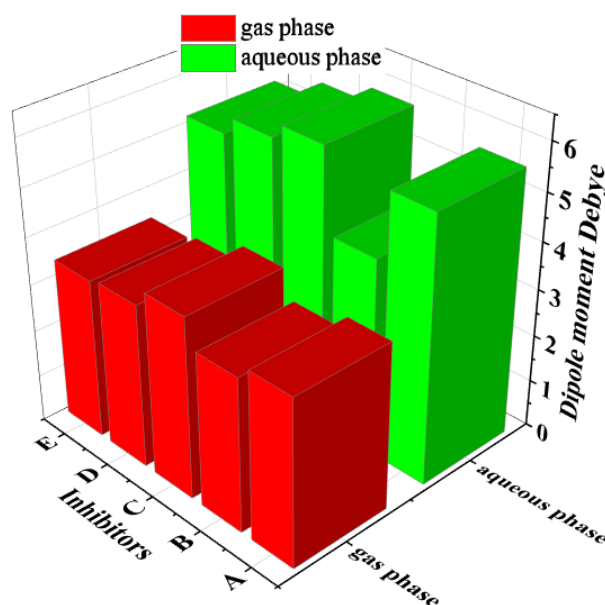


Fig. 3. Dipole moment variation among inhibitors in gas and aqueous phases

219 **Thermal properties:** The significant thermodynamic parameters for the title compounds
 such as enthalpy (H), entropy (S), free energy (ΔG) and heat capacity (Cv) was estimated
 by DFT with the 6-311++G (d, p) basis set in various temperatures. Also, Thermodynamic
 222 results derived from theoretical approaches are significant for comprehending chemical
 processes [17, 33]. The thermodynamic parameters are illustrated in Fig. 4. It was observed
 that entropy, heat capacity, and enthalpy increase as temperature rises. Whereas, free
 225 energy decreases with increasing temperatures.

Fukui function analysis: The selected inhibitors' local reactivity can be determined by
 measuring the Fukui indices of each of their atoms [34, 35]. The Fukui indices give more
 228 comprehensive information on the reactivity of the compounds under investigation. In
 general, the greatest f^- signifies the site for electrophilic assault or when the inhibitor
 receives electrons, whereas the highest f^+ indicates the site for nucleophilic attack or when
 231 the inhibitor gives electrons [36]. Tables 7 to 16 shows how condensed Fukui indices are
 used to examine a molecule's local reactivity. The most reactive locations for nucleophilic
 assault are S (1), N (1,2), and C (8) atoms for 2-mercaptobenzimidazole, benzotriazole, and
 234 2-methylbenzimidazol, respectively. suggesting a proclivity to transfer electrons to
 unoccupied molecular orbitals on the Fe surface to form a coordinating bond, whereas S (1)
 is the most reactive site for electrophilic attack for 2-mercaptobenzimidazole.

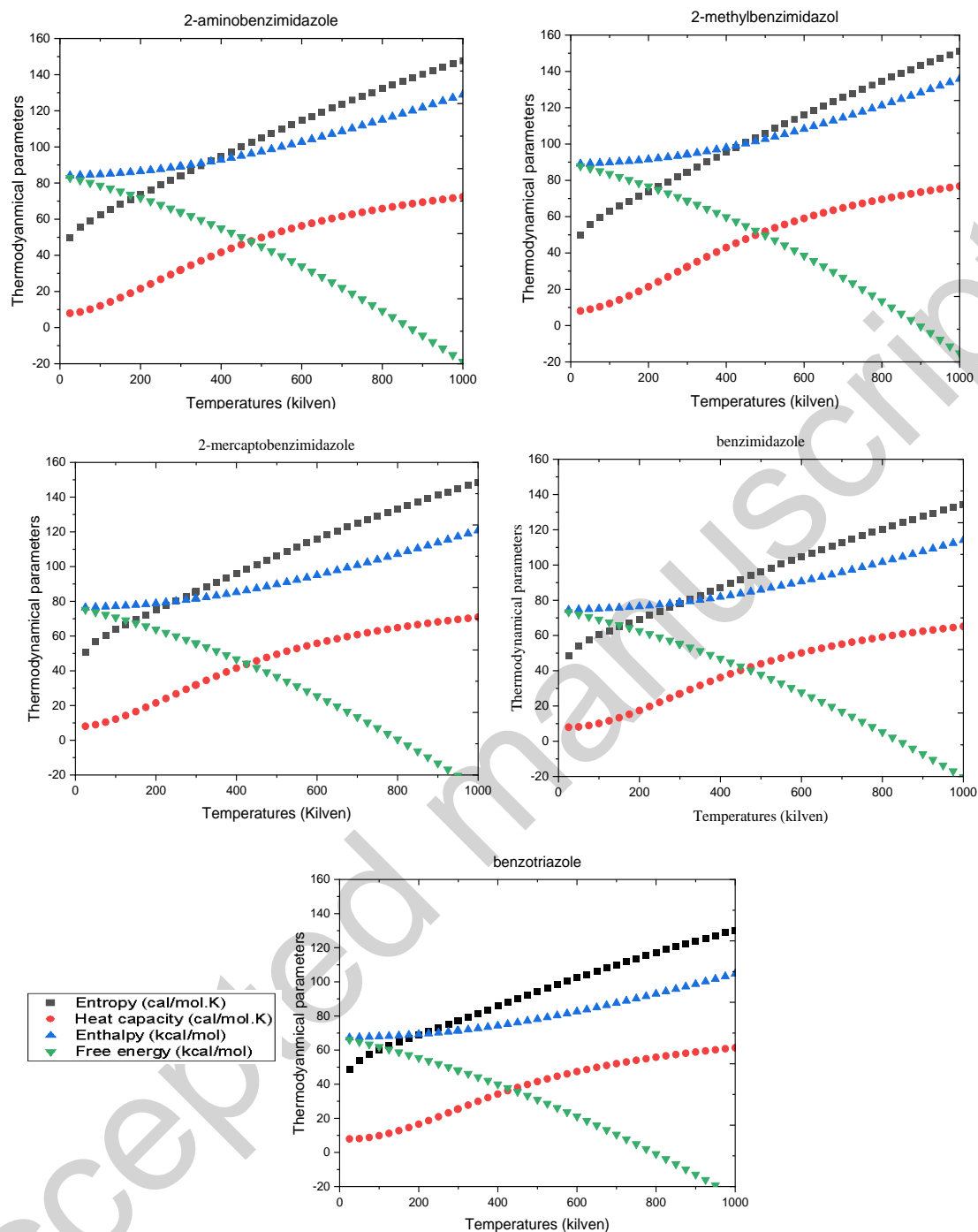


Fig. 4. Thermal properties of the title compounds

240 Table. 7. Fukui functions for 2-Aminobenzimidazole from NBO charges at 6-311++G (d, p)

Atoms	q(N)	q(N+1)	q(N-1)	F^+	F^-
N 1	-0.58996	-0.57746	-0.70082	0.0125	0.11086
N 2	-0.56464	-0.43287	-0.59576	0.13177	0.03112
N 3	-0.80844	-0.65574	-0.97046	0.1527	0.16202
C 4	0.12097	0.20784	0.07254	0.08687	0.04843
C 5	0.12258	0.18676	0.12569	0.06418	-0.00311
C 6	0.58267	0.63212	0.35004	0.04945	0.23263

C 7	-0.24503	-0.24094	-0.28288	0.00409	0.03785
C 8	-0.21101	-0.1509	-0.2324	0.06011	0.02139
C 9	-0.21949	-0.05182	-0.24441	0.16767	0.02492
C 10	-0.22075	-0.1808	-0.24233	0.03995	0.02158
H 11	0.40411	0.43501	0.30343	0.0309	0.10068
H 12	0.20626	0.24368	0.20166	0.03742	0.0046
H 13	0.21495	0.2504	0.19993	0.03545	0.01502
H 14	0.2037	0.23618	0.18807	0.03248	0.01563
H 15	0.20388	0.24095	0.1873	0.03707	0.01658
H 16	0.41046	0.43704	0.37064	0.02658	0.03982
H 17	0.38974	0.42055	0.26976	0.03081	0.11998

Table 8. Fukui functions for 2-Aminobenzimidazole from NBO charges at b2plypd3/aug-cc-pvdz

243

Atoms	q(N)	q(N+1)	q(N-1)	F^+	F^-
N 1	-0.65084	-0.63871	-0.66604	0.01213	0.0152
N 2	-0.57658	-0.41275	-0.60406	0.16383	0.02748
N 3	-0.88981	-0.74979	-0.92594	0.14002	0.03613
C 4	0.12476	0.19473	0.13692	0.06997	-0.01216
C 5	0.11303	0.16018	0.05505	0.04715	0.05798
C 6	0.61687	0.66735	0.51041	0.05048	0.10646
C 7	-0.27686	-0.26631	-0.45859	0.01055	0.18173
C 8	-0.23964	-0.16453	-0.42067	0.07511	0.18103
C 9	-0.25480	-0.10256	-0.35573	0.15224	0.10093
C 10	-0.26021	-0.24602	-0.26334	0.01419	0.00313
H 11	0.44397	0.47818	0.41136	0.03421	0.03261
H 12	0.24321	0.28347	0.18780	0.04026	0.05541
H 13	0.25420	0.29196	0.19904	0.03776	0.05516
H 14	0.24262	0.28110	0.19023	0.03848	0.05239
H 15	0.24320	0.28476	0.19419	0.04156	0.04901
H 16	0.44413	0.47700	0.41606	0.03287	0.02807
H 17	0.42276	0.46194	0.39331	0.03918	0.02945

Table 9. Fukui functions for 2-methylbenzimidazole from NBO charges at 6-311++G (d, p)

Atoms	q(N)	q(N+1)	q(N-1)	F^+	F^-
N 1	-0.59416	-0.5855	-0.61686	0.00866	0.0227
N 2	-0.49208	-0.40284	-0.54799	0.08924	0.05591
C 3	0.11621	0.17472	0.12577	0.05851	-0.00956
C 4	0.09958	0.19598	0.06398	0.0964	0.0356
C 5	0.3993	0.5393	0.26091	0.14	0.13839
C 6	-0.27407	-0.23455	-0.41101	0.03952	0.13694
C 7	-0.22864	-0.13992	-0.37335	0.08872	0.14471
C 8	-0.73878	-0.76768	-0.71958	-0.0289	-0.0192
C 9	-0.24856	-0.05646	-0.34036	0.1921	0.0918
C 10	-0.26457	-0.25528	-0.27886	0.00929	0.01429
H 11	0.44651	0.47843	0.40532	0.03192	0.04119
H 12	0.2443	0.28551	0.19435	0.04121	0.04995

H 13	0.25389	0.29342	0.20455	0.03953	0.04934
H 14	0.27929	0.30582	0.24825	0.02653	0.03104
H 15	0.25516	0.29892	0.19668	0.04376	0.05848
H 16	0.25515	0.29892	0.19669	0.04377	0.05846
H 17	0.24553	0.28283	0.19395	0.0373	0.05158
H 18	0.24593	0.28839	0.19755	0.04246	0.04838

246

Table 10. Fukui functions for 2-methylbenzimidazole from NBO charges at b2plypd3/aug-cc-pvdz

Atoms	q(N)	q(N+1)	q(N-1)	F^+	F^-
N 1	-0.60115	-0.61129	-0.62353	-0.01014	0.02238
N 2	-0.53398	-0.49499	-0.57186	0.03899	0.03788
C 3	0.13556	0.25379	0.16103	0.11823	-0.02547
C 4	0.11311	0.27059	0.07348	0.15748	0.03963
C 5	0.45637	0.61290	0.31785	0.15653	0.13852
C 6	-0.23872	-0.25220	-0.44002	-0.01348	0.20130
C 7	-0.18841	-0.16663	-0.39197	0.02178	0.20356
C 8	-0.59665	-0.62819	-0.58188	-0.03154	-0.01477
C 9	-0.20088	0.00325	-0.32246	0.20413	0.12158
C 10	-0.22189	-0.15808	-0.22284	0.06381	0.00095
H 11	0.41043	0.44382	0.38423	0.03339	0.02620
H 12	0.20493	0.24619	0.17103	0.04126	0.03390
H 13	0.21353	0.25420	0.17807	0.04067	0.03546
H 14	0.23079	0.25571	0.20842	0.02492	0.02237
H 15	0.20706	0.24835	0.16330	0.04129	0.04376
H 16	0.20705	0.24836	0.16327	0.04131	0.04378
H 17	0.20106	0.23322	0.16712	0.03216	0.03394
H 18	0.20177	0.24101	0.16678	0.03924	0.03499

249

Table 11. Fukui functions for 2-mercaptobenzimidazole from NBO charges at 6-311++G(d, p)

Atoms	q(N)	q(N+1)	q(N-1)	F^+	F^-
S 1	-0.21147	0.25286	-0.45750	0.46433	0.24603
N 2	-0.59253	-0.52023	-0.59812	0.07230	0.00559
N 3	-0.59253	-0.52023	-0.59812	0.07230	0.00559
C 4	0.13260	0.17550	0.12309	0.04290	0.00951
C 5	0.13260	0.17550	0.12309	0.0429	0.00951
C 6	-0.26392	-0.24545	-0.44032	0.01847	0.1764
C 7	-0.26392	-0.24545	-0.44032	0.01847	0.1764
C 8	0.21230	0.15003	0.12816	-0.06227	0.08414
C 9	-0.24813	-0.17228	-0.29930	0.07585	0.05117
C 10	-0.24813	-0.17228	-0.29930	0.07585	0.05117
H 11	0.46569	0.49203	0.44298	0.02634	0.02271
H 12	0.46569	0.49203	0.44298	0.02634	0.02271
H 13	0.25366	0.28419	0.21919	0.03053	0.03447
H 14	0.25366	0.28419	0.21919	0.03053	0.03447

252

H 15	0.25221	0.28481	0.21716	0.0326	0.03505
H 16	0.25221	0.28481	0.21716	0.0326	0.03505

255

Table 12. Fukui functions for 2-mercaptobenzimidazole from NBO charges at b2plypd3/aug-cc-pvdz

Atoms	q(N)	q(N+1)	q(N-1)	F^+	F^-
S 1	-0.24311	0.27773	-0.46707	0.52084	0.22396
N 2	-0.62884	-0.54632	-0.64526	0.08252	0.01642
N 3	-0.62884	-0.54632	-0.64526	0.08252	0.01642
C 4	0.14342	0.1821	0.16007	0.03868	-0.01665
C 5	0.14342	0.1821	0.16007	0.03868	-0.01665
C 6	-0.26058	-0.24911	-0.42313	0.01147	0.16255
C 7	-0.26058	-0.24911	-0.42313	0.01147	0.16255
C 8	0.27843	0.17591	0.22111	-0.10252	0.05732
C 9	-0.2449	-0.172	-0.26422	0.0729	0.01932
C 10	-0.2449	-0.172	-0.26422	0.0729	0.01932
H 11	0.47007	0.49533	0.42685	0.02526	0.04322
H 12	0.47007	0.49533	0.42685	0.02526	0.04322
H 13	0.25263	0.28144	0.18454	0.02881	0.06809
H 14	0.25263	0.28144	0.18454	0.02881	0.06809
H 15	0.25054	0.28175	0.18413	0.03121	0.06641
H 16	0.25054	0.28175	0.18413	0.03121	0.06641

Table 13. Fukui functions for Benzimidazole from NBO charges at 6-311++G (d, p)

Atoms	q(N)	q(N+1)	q(N-1)	F^+	F^-
N 1	-0.55903	-0.49233	-0.60401	0.06670	0.04498
N 2	-0.48840	-0.43388	-0.52476	0.05452	0.03636
C 3	0.12026	0.25476	0.11523	0.13450	0.00503
C 4	0.10251	0.17231	0.09986	0.06980	0.00265
C 5	-0.23584	-0.16698	-0.23749	0.06886	0.00165
C 6	-0.18982	-0.16116	-0.20594	0.02866	0.01612
C 7	-0.20154	-0.16785	-0.22276	0.03369	0.02122
C 8	0.24262	0.31933	0.24088	0.07671	0.00174
C 9	-0.21938	0.00956	-0.23469	0.22894	0.01531
H 10	0.40740	0.44433	-0.04663	0.03693	0.45403
H 11	0.20727	0.24865	0.05318	0.04138	0.15409
H 12	0.21537	0.25723	0.19955	0.04186	0.01582
H 13	0.18983	0.23288	0.05203	0.04305	0.13780
H 14	0.20400	0.24561	0.14150	0.04161	0.06250
H 15	0.20476	0.23753	0.17404	0.03277	0.03072

258

Table 14. Fukui functions for Benzimidazole from NBO charges at b2plypd3/aug-cc-pvdz

Atoms	q(N)	q(N+1)	q(N-1)	F^+	F^-
N 1	-0.62810	-0.63317	-0.65267	-0.00507	0.02457
N 2	-0.51148	-0.47351	-0.56252	0.03797	0.05104
C 3	0.12383	0.23834	0.13625	0.11451	-0.01242

C 4	0.09846	0.26597	0.07257	0.16751	0.02589
C 5	-0.27166	-0.28196	-0.44297	-0.01030	0.17131
C 6	-0.22090	-0.20116	-0.39730	0.01974	0.17640
C 7	-0.24100	-0.02990	-0.36080	0.21110	0.11980
C 8	0.23895	0.39380	0.01868	0.15485	0.22027
C 9	-0.26365	-0.20402	-0.28470	0.05963	0.02105
H 10	0.45467	0.49021	0.42548	0.03554	0.02919
H 11	0.24439	0.28894	0.21068	0.04455	0.03371
H 12	0.25415	0.29819	0.21901	0.04404	0.03514
H 13	0.23281	0.27813	0.20104	0.04532	0.03177
H 14	0.24453	0.28180	0.20800	0.03727	0.03653
H 15	0.24501	0.28833	0.20924	0.04332	0.03577

261 Table 15. Fukui functions for Benzotriazole from NBO charges at 6-311++G (d, p)

Atoms	q(N)	q(N+1)	q(N-1)	F^+	F^-
N 1	-0.24214	-0.11250	-0.35568	0.12964	0.11354
N 2	-0.03696	0.02232	-0.20572	0.05928	0.16876
C 3	0.07023	0.04386	0.06581	-0.02637	0.00442
C 4	0.11494	0.11329	0.12380	-0.00165	-0.00886
C 5	-0.17605	0.00586	-0.34877	0.18191	0.17272
C 6	-0.23122	-0.02342	-0.38865	0.20780	0.15743
C 7	-0.21743	-0.08827	-0.24576	0.12916	0.02833
C 8	-0.18287	-0.17423	-0.30127	0.00864	0.11840
H 9	0.22161	0.25652	0.18384	0.03491	0.03777
H 10	0.21330	0.24776	0.17596	0.03446	0.03734
H 11	0.20933	0.24776	0.17208	0.03843	0.03725
H 12	0.20813	0.25086	0.17123	0.04273	0.03690
N 13	-0.36095	-0.23681	-0.42099	0.12414	0.06004
H 14	0.41009	0.44700	0.37415	0.03691	0.03594

Table 16. Fukui functions for Benzotriazole from NBO charges at b2plypd3/aug-cc-pvdz

Atoms	q(N)	q(N+1)	q(N-1)	F^+	F^-
N 1	-0.24373	-0.14314	-0.41027	0.10059	0.16654
N 2	-0.02878	0.04462	-0.18979	0.07340	0.16101
C 3	0.06014	0.04226	0.08845	-0.01788	-0.02831
C 4	0.12740	0.13391	0.14712	0.00651	-0.01972
C 5	-0.19706	0.01341	-0.34087	0.21047	0.14381
C 6	-0.26492	-0.03698	-0.38601	0.22794	0.12109
C 7	-0.25609	-0.09698	-0.24802	0.15911	-0.00807
C 8	-0.21005	-0.19179	-0.30920	0.01826	0.09915
H 9	0.25322	0.27386	0.19397	0.02064	0.05925
H 10	0.24431	0.26268	0.18351	0.01837	0.06080
H 11	0.24151	0.26397	0.18196	0.02246	0.05955
H 12	0.24089	0.26552	0.17916	0.02463	0.06173
N 13	-0.41643	-0.31431	-0.49396	0.10212	0.07753
H 14	0.44960	0.48297	0.40395	0.03337	0.04565

264

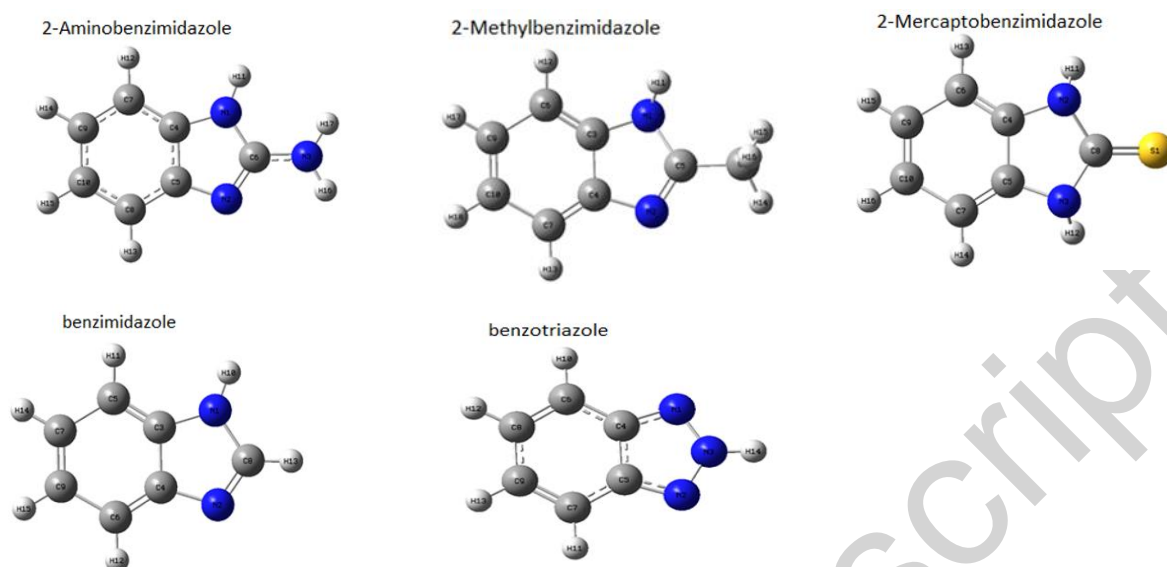


Fig. 5. Optimized molecule structures based on DFT at 6-311++G(d,p) basis set

267 Using natural bonding orbitals (NBOs), it was performed in b2plypd3/aug-cc-pvdz basis set
 for all identified molecules. It is assumed that the more negative the atomic charges of the
 adsorbed center, the more readily the atom gives its electrons to the metal/metal oxide's
 270 empty orbital. Table 8,10, 12, 14 and 16 shows that nitrogen atoms have negative charge
 centers that might give electrons to the iron surface to establish a coordinate-type
 connection, the highest negative values are bolded in the Tables 8,10, 12, 14 and 16.

273 *Monte Carlo stimulation:* The Monte Carlo simulation is often used to investigate the
 interaction between a molecule inhibitor and a metal surface [37]. This method can illustrate
 one of the most important aspects of the corrosion problem: the adsorption phenomena.
 276 The most stable adsorption sites are found on low-energy metal surfaces. In molecular
 dynamics simulations done with the adsorption locator and the Forcite code, to determine a
 feasible position for the interaction between the inhibitor and the Fe surface provided in
 279 Material Studio 7.0 software [38].

Using a Monte Carlo simulation, Fig. 6 depicts the most stable low-energy energy adsorption
 arrangement of inhibitors in the Fe (110) system of a typical energy (total energy, average
 282 total energy, van der Waals energy, electrostatic energy, and intermolecular energy. These
 properties, which include structural, conformational, vibration and state equations, cohesive
 energy, and interaction energy for a wide range of organic metal molecules, metal oxides,
 285 and metal halides, make use of a variety of solid properties such as cell unit structure, lattice
 energy, and even polymers [6]. The initial phase in this computer analysis is to optimize the
 shape of the inhibitor molecule, which will adsorb next on the iron surface with the least

288 amount of energy [39]. The Forcite computation was completed with excellent estimation accuracy utilizing the COMPASS forcefield for this reason [40].

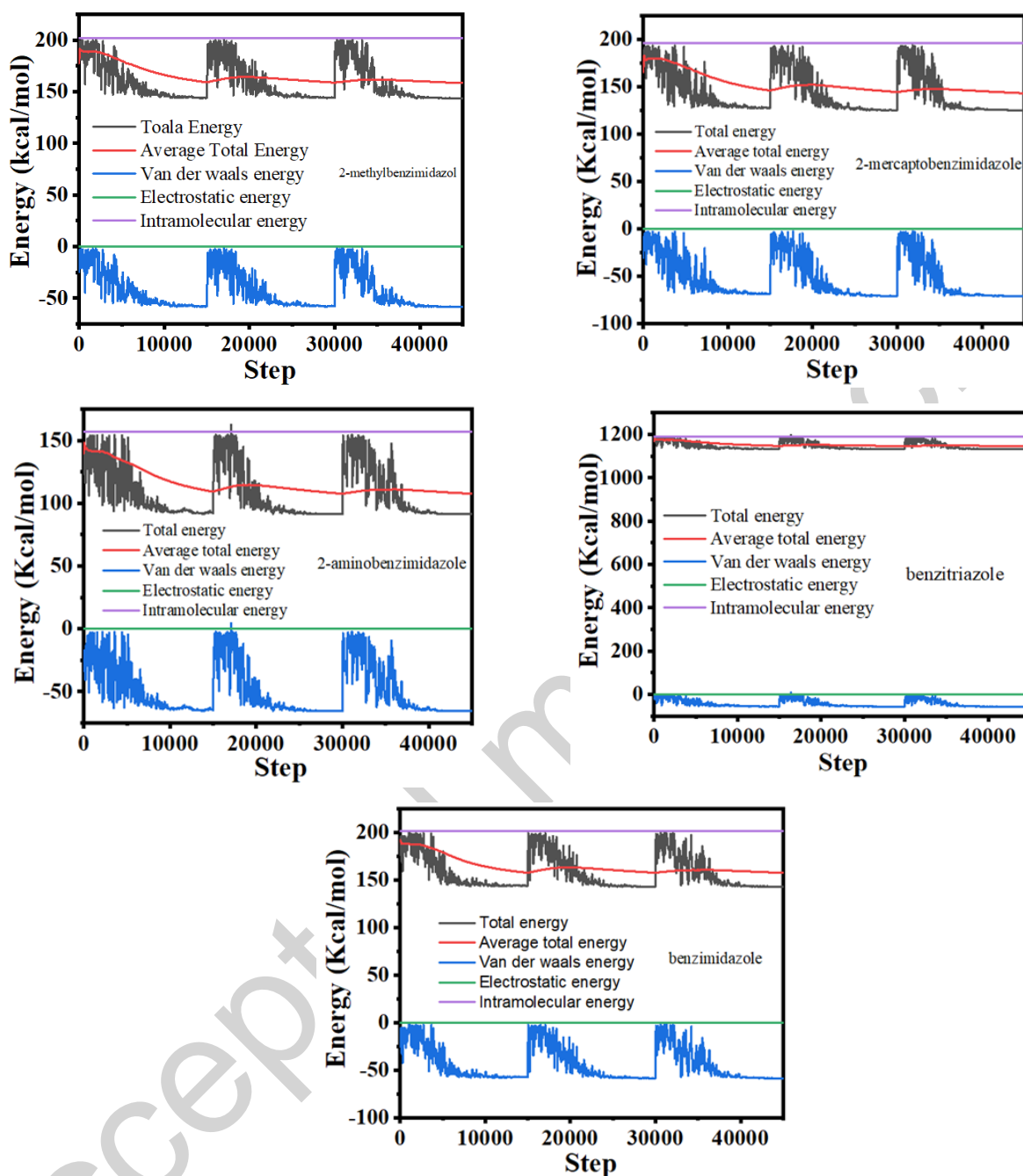


Fig. 6. Typical energy based on Monte Carlo stimulation of selected molecules

291 As a result of using the Monte Carlo method, several properties were obtained such as total
 adsorption energy, solid adsorption and deformation energies as shown in Table 17. The
 294 adsorption energy is the energy released during the adsorption process. The adsorption
 energy, is ascribed to the energy produced by the flexible adsorption compounds placed on
 the substrate. The adsorption energies of the inhibitors are estimated by summing energy
 297 of solid adsorption and adsorbent structural deformation, as shown in Table 17. Higher

negative adsorption energy values, as displayed in Fig. 7, indicate that the association between a metal and inhibitor molecules is more stable and stronger.

300

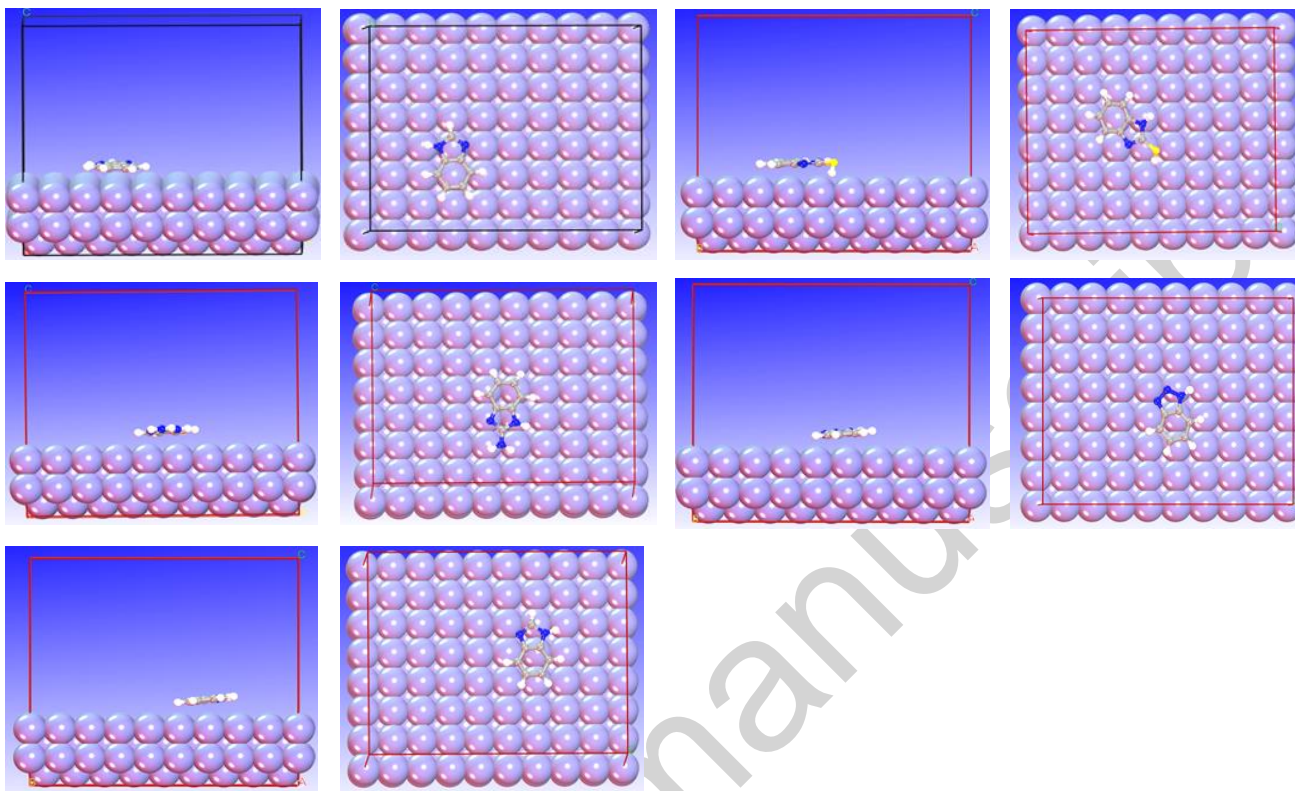


Fig. 7. Top and side views of the most stable low energy configuration for the adsorption for all selected molecules in this study

303

Table 17. The outputs and descriptors calculated by the Monte Carlo simulation for adsorption on Fe (110) (in kcal mol⁻¹) and experimental inhibition efficiency [6]

Inhibitors	Total energy	Adsorption energy	Rigid adsorption energy	Deformation energy	dE_{ad}/dN_i	% IE
2-methyl benzimidazole (MBIH)	143.58452186	-58.65350403	-58.6535040	-3.764995×10 ⁻⁹	-58.6535040	80
2-mercapto benzimidazole (2-CH ₃ -BI)	124.73065649	-71.76095653	-71.7609565	-1.234270×10 ⁻⁹	-71.7609565	96.39
2-amino benzimidazole (2-ABI)	95.84806853	-43.17668955	-43.1766895	-7.105427×10 ⁻¹³	-43.1766895	42.45
Benzotriazole (BTA)	1.134599e+003	-53.51120229	-53.5112022	-1.032276×10 ⁻¹⁰	-53.5112022	-
Benzimidazole (BIM)	145.57694973	-56.04159478	-56.0415947	7.958079×10 ⁻³	-56.0415947	56.21

306

CONCLUSIONS

The present study on the inhibition efficiency 2-aminobenzimidazole, 2-methylbenzimidazol, 2-mercaptobenzimidazole and benzimidazole in combination with benzotriazole has lead us

309 2-methylbenzimidazol was the most efficient inhibitor for iron metal in gas and solvent medium.

The calculation of chemical reactivity parameters shows that the inhibition efficiency follows
312 the order 2-methylbenzimidazol > benzotriazole > 2-aminobenzimidazole > 2-mercapto-
benzimidazole > benzimidazole.

Our calculations using Fukui function predicted the nucleophilic and electrophilic attacking
315 sites of the inhibitors. The results of quantum chemical computations and experimental
investigations were in a good agreement.

REFERENCES

1. Wang, N., Xiong, D., Deng, Y., Shi, Y., Wang, K. (2015) Mechanically robust superhydrophobic steel surface with anti-icing, UV-durability, and corrosion resistance properties. *ACS Appl. Mater. Interfaces*, **7**, 6260-6272. <https://doi.org/10.1021/acsami.5b00558>
2. Qadr, H.M. (2021) A molecular dynamics study of temperature dependence of the primary state of cascade damage processes. *Russ. J. Non-Ferr.*, **62**, 561-567. <https://doi.org/10.3103/S1067821221050096>
3. Balamurugan, A., Rajeswari, S., Balossier, G., Rebelo, A.H.S., Ferreira, J.M.F. (2008) Corrosion aspects of metallic implants - An overview. *Corros. Mater.*, **59**, 855-869. <https://doi.org/10.1002/maco.200804173>
4. Qadr, H.M. (2020) Effect of ion irradiation on the mechanical properties of high and low copper. *At. Indones.*, **46**, 47-51. <https://doi.org/10.17146/aij.2020.923>
5. Ahamed, M.R., Narren, S.F., Sadiq, A.S. (2013) Synthesis of 2-mercaptobenzimidazole and some of its derivatives. *ANJS.*, **16**, 77-83. <https://doi.org/10.22401/JNUS.16.2.11>
6. Liu, L., Lu, S., Wu, Y.Q., Xie, J.Y., Xing, J. (2020) Corrosion inhibition behavior of four benzimidazole derivatives and benzotriazole on copper surface. *Anti-Corros. Methods Mater.*, **67**, 565-574. <https://doi.org/10.1108/ACMM-12-2019-2235>
7. Altaf, M., Yamin, N., Muhammad, G., Raza, M.A., Shahid, M., *et al.* (2021) Electroanalytical techniques for the remediation of heavy metals from wastewater. *Water Pollution and Remediation: Heavy Metals*, 471-511. https://doi.org/10.1007/978-3-030-52421-0_14
8. Gupta, V.K., Ali, I. (2013) *Environmental water: advances in treatment, remediation and recycling*, 2nd Ed., Elsevier, Oxford, UK. <https://doi.org/10.1016/B978-0-444-59399-3.00008-8>

9. Qadr, H.M. (2021) Pressure effects on stopping power of alpha particles in argon gas. *Phys. Part. Nucl.*, **18**, 185-189. <https://doi.org/10.1134/S1547477121020151>
10. Tan, Y., Leonhard, M., Moser, D., Ma, S., Schneider-Stickler, B. (2019) Antibiofilm efficacy of curcumin in combination with 2-aminobenzimidazole against single-and mixed-species biofilms of *Candida albicans* and *Staphylococcus aureus*. *Colloids Surf. B: Biointerfaces.*, **174**, 28-34. <https://doi.org/10.1016/j.colsurfb.2018.10.079>
11. Song, D., Ma, S. (2016) Recent development of benzimidazole-containing antibacterial agents. *Chem.Med.Chem.*, **11**, 646-659. <https://doi.org/10.1002/cmdc.201600041>
12. Briguglio, I., Piras, S., Corona, P., Gavini, E., Nieddu, M., et al. (2015) Benzotriazole: An overview on its versatile biological behavior. *Eur. J. Med. Chem.*, **97**, 612-648. <https://doi.org/10.1016/j.ejmech.2014.09.089>
13. Pustuła, K., Płonka, A., Makowski, M. (2018) Thermal decomposition of oxetan-2-one molecule in the light of DFT and CASPT2 modelling. *Comput. Theor. Chem.*, **1140**, 98-103. <https://doi.org/10.1016/j.comptc.2018.07.020>
14. Frisch, A. (2009) Gaussian 09W Reference. Wallingford, USA, 25 p, **470**.
15. Cammi, R., Mennucci, B. (1999) Linear response theory for the polarizable continuum model. *J. Chem. Phys.*, **110**, 9877-9886. <https://doi.org/10.1063/1.478861>
16. Hussein, Y.T., Azeez, Y.H. (2021) DFT analysis and in silico exploration of drug-likeness, toxicity prediction, bioactivity score, and chemical reactivity properties of the urolithins. *J. Biomol. Struct. Dyn.*, 1-10. <https://doi.org/10.1080/07391102.2021.2017350>
17. Qadr, H.M., Mamand, D.M. (2021) Molecular structure and density functional theory investigation corrosion inhibitors of some oxadiazoles. *J. Bio- Tribo-Corros.*, **7**, 140. <https://doi.org/10.1007/s40735-021-00566-9>
18. Mamand, D.M., Rasul, H.H., Omer, P.K., Qadr, H.M. (2022) Theoretical and experimental investigation on ADT organic semiconductor in different solvents. *Condens. Matter Interphases.*, **24**, 227-242. <https://doi.org/10.17308/kcmf.2022.24/9263>
19. Outirite, M., Lagrenée, M., Lebrini, M., Traisnel, M., Jama, C., et al. (2010) ac impedance, X-ray photoelectron spectroscopy and density functional theory studies of 3, 5-bis (n-pyridyl)-1, 2, 4-oxadiazoles as efficient corrosion inhibitors for carbon steel surface in hydrochloric acid solution. *Electrochim. Acta.*, **55**, 1670-1681. <https://doi.org/10.1016/j.electacta.2009.10.048>
20. Mamand, D.M., Anwer, T.M.K., Qadr, H.M. (2022) Theoretical investigation on corrosion inhibition effect of oxadiazole: DFT calculations. *Oxid. Commun.*, **45**, 600-627.

21. Ju, H., Ding, L., Sun, C., Chen, J.-j. (2015) Quantum chemical study on the corrosion inhibition of some oxadiazoles. *Adv. Mater. Sci. Eng.*, **2015**.
<https://doi.org/10.1155/2015/519606>
22. Demissie, E.G., Kassa, S.B., Woyessa, G.W. (2014) Quantum chemical study on corrosion inhibition efficiency of 4-amino-5-mercapto-1, 2, 4-triazole derivatives for copper in HCl solution. *Int. J. Sci. Eng. Res.*, **5**, 304.
<https://doi.org/10.14299/ijser.2014.06.001>
23. Mamand, D. (2019) Determination the band gap energy of poly benzimidazo-benzophenanthroline and comparison between HF and DFT for three different basis sets. *J. Phys. Chem. Funct. Mater.*, **2**, 32-36.
24. Zheng, X., Zhang, S., Gong, M., Li, W. (2014) Experimental and theoretical study on the corrosion inhibition of mild steel by 1-octyl-3-methylimidazolium L-prolinate in sulfuric acid solution. *Ind. Eng. Chem. Res.*, **53**, 16349-16358.
<https://doi.org/10.1021/ie502578q>
25. Djenane, M., Chafaa, S., Chafai, N., Kerkour, R., Hellal, A. (2019) Synthesis, spectral properties and corrosion inhibition efficiency of new ethyl hydrogen [(methoxyphenyl)(methylamino) methyl] phosphonate derivatives: Experimental and theoretical investigation. *J. Mol. Struct.*, **1175**, 398-413.
<https://doi.org/10.1016/j.molstruc.2018.07.087>
26. Chen, X., Chen, Y., Cui, J., Li, Y., Liang, Y., *et al.* (2021) Molecular dynamics simulation and DFT calculation of “green” scale and corrosion inhibitor. *Comput. Mater. Sci.*, **188**, 110229. <https://doi.org/10.1016/j.commatsci.2020.110229>
27. Singh, P., Srivastava, V., Quraishi, M.A. (2016) Novel quinoline derivatives as green corrosion inhibitors for mild steel in acidic medium: electrochemical, SEM, AFM, and XPS studies. *J. Mol. Liq.*, **216**, 164-173. <https://doi.org/10.1016/j.molliq.2015.12.086>
28. Kaya, S., Kaya, C., Islam, N. (2016) The nucleophilicity equalization principle and new algorithms for the evaluation of molecular nucleophilicity. *Comput. Theor. Chem.*, **1080**, 72-78. <https://doi.org/10.1016/j.comptc.2016.02.006>
29. Khaled, K.F. (2011) Experimental and computational investigations of corrosion and corrosion inhibition of iron in acid solutions. *J. Appl. Electrochem.*, **41**, 277-287.
<https://doi.org/10.1007/s10800-010-0235-2>
30. Goulart, C.M., Esteves-Souza, A., Martinez-Huitle, C.A., Rodrigues, C.J.F., Maciel, M.A.M., *et al.* (2013) Experimental and theoretical evaluation of semicarbazones and thiosemicarbazones as organic corrosion inhibitors. *Corros. Sci.*, **67**, 281-291.
<https://doi.org/10.1016/j.corsci.2012.10.029>

31. Qadr, H.M., Mamand, D. (2022) A Review on DPA for computing radiation damage simulation. *J. Phys. Chem. Funct. Mater.*, **5**, 30-36.
<https://doi.org/10.54565/jphcfum.1027393>
32. Mamand, D. (2019) Theoretical calculations and spectroscopic analysis of gaussian computational examination-NMR, FTIR, UV-Visible, MEP on 2, 4, 6-Nitrophenol. *J. Phys. Chem. Funct. Mater.*, **2**, 77-86.
33. El Faydy, M., Galai, M., El Assyry, A., Tazouti, A., Touir, R., *et al.* (2016) Experimental investigation on the corrosion inhibition of carbon steel by 5-(chloromethyl)-8-quinolinol hydrochloride in hydrochloric acid solution. *J. Mol. Liq.*, **219**, 396-404.
<https://doi.org/10.1016/j.molliq.2016.03.056>
34. Hadisaputra, S., Purwoko, A.A., Savalas, L.R.T., Prasetyo, N., Yuanita, E., *et al.* (2020) Quantum chemical and Monte Carlo simulation studies on inhibition performance of caffeine and its derivatives against corrosion of copper. *Coatings.*, **10**, 1086.
<https://doi.org/10.3390/coatings10111086>
35. Erdoğan, Ş., Safi, Z.S., Kaya, S., Işın, D.Ö., Guo, L., *et al.* (2017) A computational study on corrosion inhibition performances of novel quinoline derivatives against the corrosion of iron. *J. Mol. Struct.*, **1134**, 751-761. <https://doi.org/10.1016/j.molstruc.2017.01.037>
36. Frenkel, D., Smit, B., Ratner, M.A. (1996) *Understanding molecular simulation: From algorithms to applications*, Academic press San Diego.
37. Mamand, D.M., Qadr, H.M. (2021) Comprehensive spectroscopic and optoelectronic properties of bbl organic semiconductor. *Prot. Met. Phys. Chem. Surf.*, **57**, 943-953.
<https://doi.org/10.1134/S207020512105018X>
38. Guo, L., Zhu, S., Zhang, S. (2015) Experimental and theoretical studies of benzalkonium chloride as an inhibitor for carbon steel corrosion in sulfuric acid. *J. Ind. Eng. Chem.*, **24**, 174-180. <https://doi.org/10.1016/j.jiec.2014.09.026>
39. Mamand, D.M., Anwer, T.M.K., Qadr, H.M., Mussa, C.H. (2022) Investigation of spectroscopic and optoelectronic properties of phthalocyanine molecules. *Russ. J. Gen. Chem.*, **92**, 1827-1838. <https://doi.org/10.1134/S1070363222090249>
40. Mamand, D.M., Qadr, H.M. (2022) Density functional theory and computational simulation of the molecular structure on corrosion of carbon steel in acidic media of some amino acids. *Russ. J. Phys. Chem. A.*, **96**, 2155-2165.
<https://doi.org/10.1134/S0036024422100193>